

Article

# Enabling Quick Response to Nitrogen Dioxide at Room Temperature and Limit of Detection to Ppb Level by Heavily n-Doped Graphene Hybrid Transistor

Si-Wei Song <sup>†</sup>, Qian-Min Wang <sup>†</sup>, Miao Yu, Zhi-Yuan Tian  and Zhi-Yong Yang <sup>\*</sup>

School of Chemical Science, University of Chinese Academy of Sciences, 19A Yuquanlu, Beijing 100049, China

<sup>\*</sup> Correspondence: yangzhiyong@ucas.ac.cn<sup>†</sup> These authors contributed equally to this work.

**Abstract:** Sensitive detection of nitrogen dioxide (NO<sub>2</sub>) is of significance in many areas for health and environmental protections. In this work, we developed an efficient NO<sub>2</sub> sensor that can respond within seconds at room temperature, and the limit of detection (LOD) is as low as 100 ppb. Coating cyano-substituted poly(p-phenylene vinylene) (CN-PPV) films on graphene (G) layers can dope G sheets effectively to a heavy *n* state. The influences of solution concentrations and annealing temperatures on the *n*-doping effect were investigated in detail. The CN-PPV-G transistors fabricated with the optimized parameters demonstrate active sensing abilities toward NO<sub>2</sub>. The *n*-doping state of CN-PPV-G is reduced dramatically by NO<sub>2</sub>, which is a strong *p*-doping compound. Upon exposure to 25 ppm of NO<sub>2</sub>, our CN-PPV-G sensors react in 10 s, indicating it is almost an immediate response. LOD is determined as low as 100 ppb. The ultrahigh responding speed and low LOD are not affected in dry air. Furthermore, cycling use of our sensors can be realized through simple annealing. The superior features shown by our CN-PPV-G sensors are highly desired in the applications of monitoring the level of NO<sub>2</sub> in situ and setting immediate alarms. Our results also suggest that transfer curves of transistors can react very promptly to the stimulus of target gas and, thus, are very promising in the development of fast-response sensing devices although the response values may not reach maximum as a tradeoff.

**Keywords:** nitrogen dioxide; graphene; sensor; field effect transistor; poly(p-phenylene vinylene)



**Citation:** Song, S.-W.; Wang, Q.-M.; Yu, M.; Tian, Z.-Y.; Yang, Z.-Y. Enabling Quick Response to Nitrogen Dioxide at Room Temperature and Limit of Detection to Ppb Level by Heavily n-Doped Graphene Hybrid Transistor. *Molecules* **2023**, *28*, 5054. <https://doi.org/10.3390/molecules28135054>

Academic Editor: Chongjun Zhao

Received: 19 May 2023

Revised: 13 June 2023

Accepted: 20 June 2023

Published: 28 June 2023



**Copyright:** © 2023 by the authors. Licensee MDPI, Basel, Switzerland. This article is an open access article distributed under the terms and conditions of the Creative Commons Attribution (CC BY) license (<https://creativecommons.org/licenses/by/4.0/>).

## 1. Introduction

Nitrogen dioxide (NO<sub>2</sub>) is notorious for its severe threats to our health and environment. For instance, our teeth, respiratory and cardiovascular systems could be hurt seriously by low concentration NO<sub>2</sub>, and the acid rain formed by NO<sub>2</sub> dissolving in water leads to detrimental damages to both the aquatic and terrestrial ecosystems [1]. Therefore, great efforts have been devoted to fabricating efficient sensors that can quickly respond to a low level of NO<sub>2</sub>. Other properties of NO<sub>2</sub> sensors, such as operation temperature, reliabilities and recovery time, are also very important for realizing successful applications.

Quite a lot of material was used in NO<sub>2</sub> sensing. Semiconducting metal oxides (MOXs) demonstrate excellent sensitivity in NO<sub>2</sub> detection [1,2]. However, most of them need work at above room temperature (RT) [3,4]. Studies on graphene (G) materials stimulated the rapid developments of other two-dimensional (2D) materials [5]. Very soon these materials were tested as NO<sub>2</sub>-sensing candidates because of their outstanding electrical properties, very high surface-to-volume ratio, excellent stability and flexibility [3,6–11]. Among all of the 2D sheets, preparation of G materials is most convenient due to the varied, well-developed synthesis approaches with low cost. Reduced G oxides (RGOs) are produced mainly in solution, which facilitates their compounding with nano MOXs that are prepared usually in liquid as well. Thus, numerous MOX–RGO hybrids were fabricated

with the anticipation of combining the advantages of two kinds of components, including ZnO–RGO, SnO<sub>2</sub>–RGO, Cu<sub>2</sub>O–RGO [12–16]. Most of MOX–RGO films demonstrate improved sensing performances in one or several aspects. Besides inorganic components, organic compound–RGO or GO hybrids, such as dopamine, poly(styrene sulfonic acid) sodium salt and amyloid nanofibril, manifest remarkable NO<sub>2</sub> sensing capabilities as well [17–19]. RGO with other 2D materials, mainly MoS<sub>2</sub>, can also realize quick response or RT operation [20,21]. In comparison with GO or RGO materials, G layers fabricated through chemical vapor deposition or mechanical cleavage from highly oriented pyrolytic graphite have better uniform electronic properties. The sensing capabilities of pristine G layers can be promoted by assistive approaches, for instance, post modification by O<sub>3</sub> or lithography, or under UV illumination or heating [3,10,22–25]. Most current NO<sub>2</sub> sensors rely on the changing of resistance. In contrast to the widely studied resistance devices, NO<sub>2</sub> sensors based on field effect transistor (FET) have not been paid enough attention although the detection of a single NO<sub>2</sub> molecule was reported on a G FET [26]. Gate bias ( $V_g$ ) in FET is another external option for tuning the sensor activities besides the above mentioned illumination or heating, etc. Poly(p-phenylene vinylene) (PPV) is a kind of conjugated polymer. Its derivatives were fabricated into in kinds of electronic devices, such as FET, solar cells and light-emitting diodes [27,28]. In addition to electronics, they were used in gas detecting areas after forming hybrid films with other materials including porous silicon, carbon nanotubes, ZnO nanorods [27,28].

Here, we report an effective NO<sub>2</sub> sensor that can respond to 25 ppm of target molecules within 10 s at room temperature, and the limit of detection (LOD) is as low as 100 ppb. Quick response and low LOD are not affected in dry air. Furthermore, cycle use of our sensors can be realized through simple heating treatment. Coating cyano-substituted poly(p-phenylene vinylene) (CN-PPV) on G sheets shifts the minimum point (MP) of FET transfer curves of hybrid films to a very negative  $V_g$  value, revealing the giant *n*-doping effect of CN-PPV to G (*n*-doping effect means the Fermi level of G is shifted toward above the G Dirac point). NO<sub>2</sub> is well known for its strong *p*-doping abilities to G layers (*p*-doping effect means the Fermi level of G is shifted toward below the G Dirac point). As a consequence, exposing to NO<sub>2</sub> leads to the dramatic reduction of the *n*-doping state of CN-PPV–G hybrid films. The transfer curves of transistors, usually referring as the variation of the current (*I*) between drain (*d*) and source (*s*) electrode with  $V_g$ , are able to sensitively collect the changing of the G doping state before and after NO<sub>2</sub> exposure. Thus, relying on the vigorous alterations of the transfer curves of CN-PPV–G transistors, efficient NO<sub>2</sub> detection with high responding speed is realized. The results in this report demonstrate the promising detection abilities based on the field effect of 2D materials and provide valuable supports for developing new types of high performance gas sensors.

## 2. Results and Discussions

### 2.1. Structural Characterizations of CN-PPV–G Films

G sheets after transfer onto SiO<sub>2</sub>/Si substrate were characterized by Raman spectroscopy (Figure 1a). The spectroscopy shows typical G and 2D signals. The D peak at 1350 cm<sup>−1</sup>, indicating defects and fractures of G layers, is rather weak, suggesting the quality of G layers is very high. The average thickness estimated from the G and 2D peaks is around 1–2 layers, which is further confirmed by the following characterizations of atomic force microscopy (AFM, Figures 2 and S1) and scanning electron microscopy (SEM, Figures 3 and S2). In many practical applications of G electronic devices, the rigid single layer of G may not show best performances because its structure is more easily destroyed during the transfer and device fabrication processes and its electronic properties tend to be sensitively affected by the charges trapped at the interface of substrates. Therefore, multi-layer G sheets were used. Highly conductive FET devices, showing intrinsic properties of pristine G sheets, were acquired after thermal annealing at 423 K.

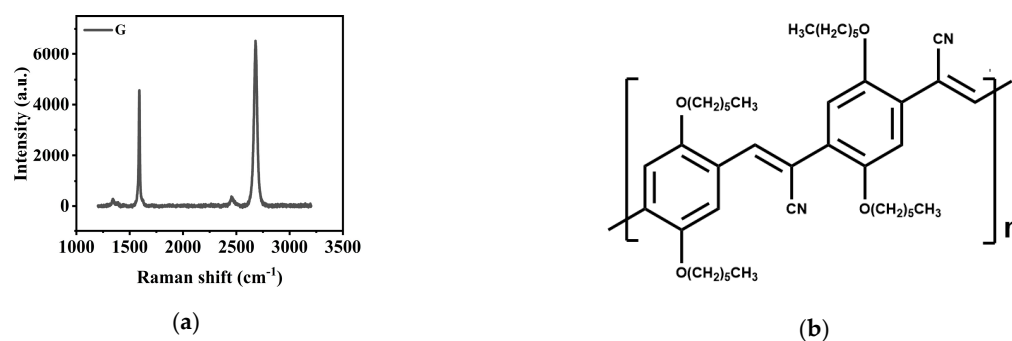


**Figure 1.** (a) Raman spectroscopy of G sheets; (b) illustration of chemical structure of CN-PPV.

The doping effect of CN-PPV (Figure 1b) to G is related to both solution concentration and temperature of thermal annealing. Therefore, the CN-PPV-G films prepared from different concentrations and annealed at varied temperatures were characterized in detail. Surface topography of CN-PPV-G hybrid films was firstly investigated through AFM (Figures 2 and S1). After casting CN-PPV film from low concentration solution ( $0.01 \text{ mg mL}^{-1}$ , Figure S1a), G ripples and wrinkles, which appear as thin bright lines, and hexagonal bilayer areas can still be recognized in AFM images, indicating the CN-PPV film is extremely thin and may not cover the whole surface of G. Thermal annealing at 373 K, 393 K and 423 K has no obvious effect on forming continuous film. Increasing the concentration to  $1 \text{ mg mL}^{-1}$  (Figure S1b), ripples and wrinkles of G sheets are not completely covered yet. When the solution was further promoted to  $5 \text{ mg mL}^{-1}$  (Figure 2), the information from G sheets had totally disappeared. Meantime, large clusters were observed in the RT samples. Dense, continuous film with much lower surface roughness was formed via thermal treatments. With the largest concentration ( $20 \text{ mg mL}^{-1}$ ), thick film was formed in the as-casted samples (Figure S1c). The morphology of this sample was smoothed apparently through thermal treatments as well. From the AFM characterizations on the samples prepared from different concentrations and annealed at three temperatures, it can be seen that thermal annealing has obvious effects on improving the qualities of CN-PPV films fabricated from dense solutions ( $5 \text{ mg mL}^{-1}$  and  $20 \text{ mg mL}^{-1}$ ) because large clusters were reduced and films were smoothed apparently through annealing.

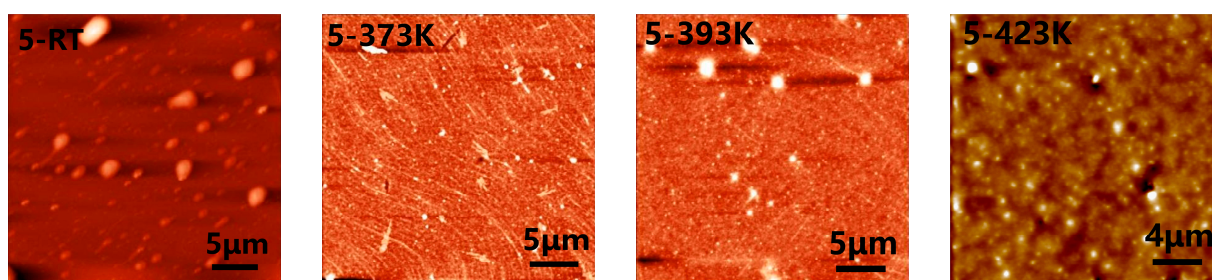


**Figure 2.** AFM topography images of CN-PPV-G films prepared with the solution of  $5 \text{ mg mL}^{-1}$  before and after 1 h thermal annealing at 373 K, 393 K and 423 K.

SEM micrographs collected on the CN-PPV-G films give similar results with AFM data overall. Only very thin CN-PPV film is formed at low concentrations ( $0.01 \text{ mg mL}^{-1}$  and  $1 \text{ mg mL}^{-1}$ ) as the multilayer areas (some are pointed out by arrows in Figure S2a,b) are disclosed clearly. For the RT samples cast from dense solutions ( $5 \text{ mg mL}^{-1}$  and  $20 \text{ mg mL}^{-1}$ ), large clusters appear (see the inserted zoom-in images), and films are very rough (Figures 3 and S2c). Annealing treatments have a significant effect on improving the qualities of these films as it can be seen that both clusters and surface roughness are apparently reduced.

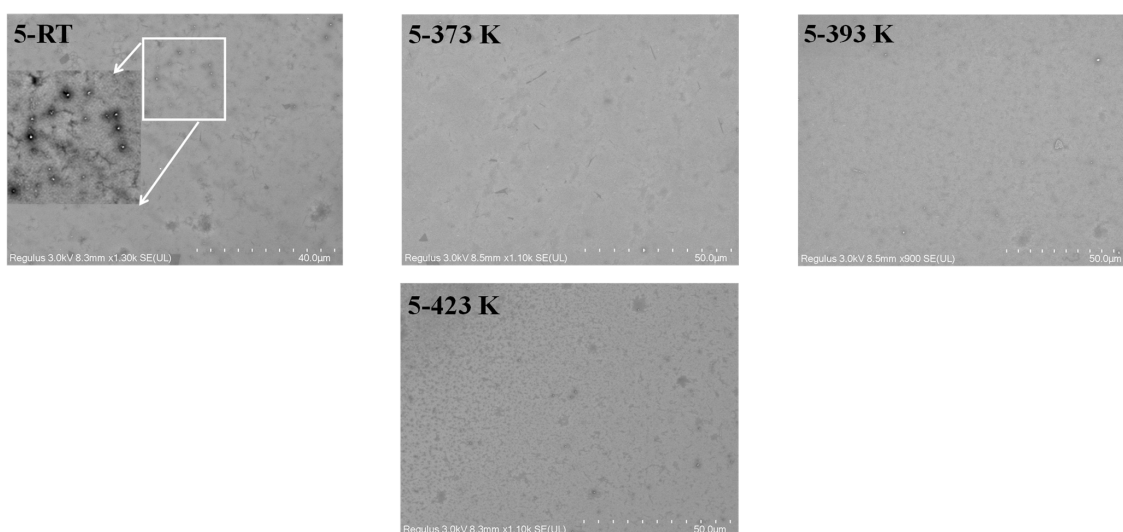


**Figure 3.** SEM images of CN-PPV-G films prepared with the solution of  $5 \text{ mg mL}^{-1}$  before and after 1 h thermal annealing at 373 K, 393 K and 423 K. Contrast and brightness of zoom-in images were post adjusted to clearly show the topographical target, which is not easily recognized in the small-size original micrographs.

After finishing the analysis on the surface topography of CN-PPV-G samples through AFM and SEM imaging, the stacking of CN-PPV was probed further by grazing-incident wide angle X-ray scattering (GIWAXS) technique. GIWAXS images (Figures 4 and S3) have no observable patterns in the  $xy$  direction, suggesting CN-PPV lacks long-range ordered in-plane arrangement; while in the  $z$  direction, diffraction signals are rather clear. In the fitting profiles (Figure S4), the peak ( $P_1$ ) corresponding to the second dot in the  $z$  direction of GIWAXS patterns suggests an interplanar distance of 1.9 nm, implying part of CN-PPV adopts an edge-on orientation in the out of plane direction. (The first dot in the  $z$  direction of each pattern is not a signal that can be reasonably generated by our CN-PPV-G films, so we discarded the corresponding peak in the fitting profiles). The GIWAXS characterizations suggest CN-PPV films are quasi amorphous, and post annealing treatments have no observable effect on forming ordered arrangement. The Raman spectroscopy of thin CN-PPV-G films prepared from  $0.01 \text{ mg mL}^{-1}$  solution detects the signals from both G substrate and CN-PPV component (Figure S5). Multi peaks generated by CN-PPV are rather complicated. Some of them overlap with the peaks of G substrate. When the thickness of CN-PPV film increases with the solution concentration, its strong fluorescence makes Raman analysis unfeasible because the Raman signals are drowned in background completely.

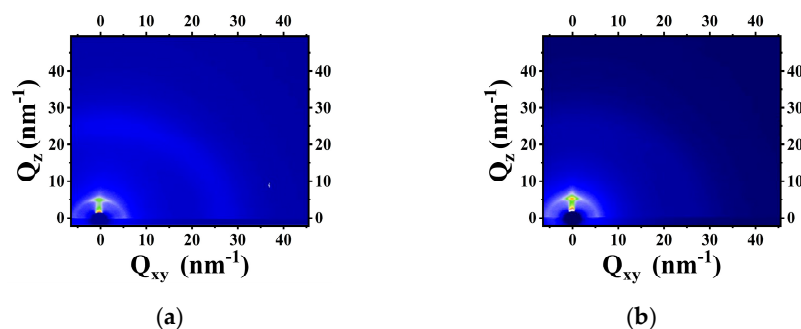


**Figure 4.** (a,b) GIWAXS patterns collected on CN-PPV-G films prepared from  $5 \text{ mg mL}^{-1}$  before and after annealed 1 h at 423 K, respectively. The first dot in the  $z$  direction of each image is not a signal that can be reasonably generated by our CN-PPV-G films, so we discarded the corresponding peak in the fitting profiles (Figure S4).

## 2.2. Doping Effect of CN-PPV to G Layers with Different Solution Concentrations and Annealing Temperatures

CN-PPV has a significant *n*-doping effect to G sheets (Figure 5). Before annealing, MP on the transfer curves of pristine G sheets and CN-PPV-G prepared from 0.01 mg mL<sup>-1</sup> solution had not been detected even at  $V_g = 60$  V (Figure 5a), which means the Fermi level ( $E_f$ ) of these two samples is lower than 0.252 eV (the  $E_f$  position is estimated to be at 0.252 eV below MP if  $V_g = 60$  V, according to the equation given in the experimental section). When the concentration of solution increases from 1 mg mL<sup>-1</sup>, 5 mg mL<sup>-1</sup> to 20 mg mL<sup>-1</sup>, MP gradually shifts from around  $V_g = 60$  V,  $V_g = 51$  V to  $V_g = 35$  V, respectively (Figures 5a and 6a), revealing the up-movement of  $E_f$  (Figure 6b) and *n*-doping tendency of CN-PPV to G sheets. At  $V_g = 0$  V,  $I_{ds}$  reading from the transfer curves in Figure 5a decreases as  $I_{ds}$  (0.01 mg mL<sup>-1</sup>) >  $I_{ds}$  (1 mg mL<sup>-1</sup>) >  $I_{ds}$  (5 mg mL<sup>-1</sup>) >  $I_{ds}$  (G) >  $I_{ds}$  (20 mg mL<sup>-1</sup>). The  $I_{ds}$  values in the output data obtained at  $V_g = 0$  V (Figure S6a) confirm this tendency perfectly. Before annealing, all the samples are in *p*-doping state.

After annealing at 373 K, MP of all samples was displaced to a left position in comparison with the corresponding one in the as-casted samples because of the desorption of *p*-doping substances such as O<sub>2</sub> and H<sub>2</sub>O in the films (Figures 5b and 6a). MP of G and CN-PPV-G casted from 0.01 mg mL<sup>-1</sup> solution is at  $V_g = 45$  V and  $V_g = 32$  V, respectively, implying  $E_f$  of these two samples is still much lower than the MP position (Figure 6b).  $E_f$  of the CN-PPV-G deposited from 1 mg mL<sup>-1</sup> solution is roughly at MP position. For the samples from denser solutions, their MPs are located at negative  $V_g$  range (Figures 5b and 6a), revealing their  $E_f$  locales above MP (Figure 6b). Thus, their *n*-doping state is disclosed clearly.  $I_{ds}$  values given by the transfer (Figure 5b) and output curves (Figure S6b) demonstrate the same sequence:  $I_{ds}$  (G) >  $I_{ds}$  (0.01 mg mL<sup>-1</sup>) >  $I_{ds}$  (5 mg mL<sup>-1</sup>) >  $I_{ds}$  (20 mg mL<sup>-1</sup>) >  $I_{ds}$  (1 mg mL<sup>-1</sup>). After annealing at 373 K, CN-PPV-G (1 mg mL<sup>-1</sup>) is a critical point ( $E_f$  roughly overlapping with MP), the samples prepared from denser solution are in a *n*-doping state whereas pristine G and CN-PPV-G from lower concentration (0.01 mg mL<sup>-1</sup>) are still in a *p*-doping state (Figure 6).

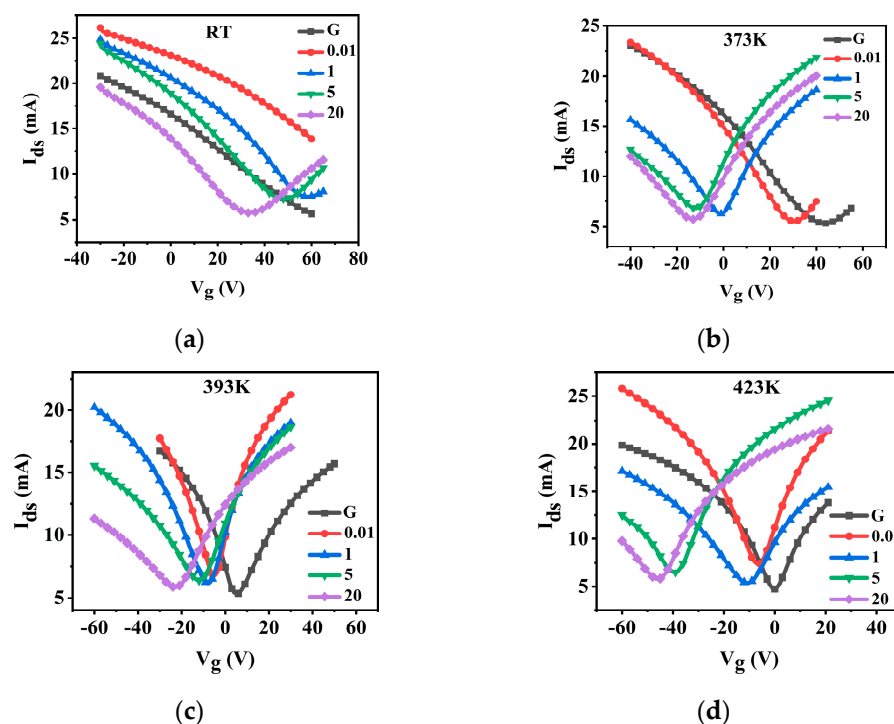


**Figure 5.** Transfer curves ( $V_{ds} = 1$  V) of pristine G and CN-PPV-G samples casted from different concentrations before (a) and after annealing 1 h at 373 K (b), 393 K (c) and 423 K (d).

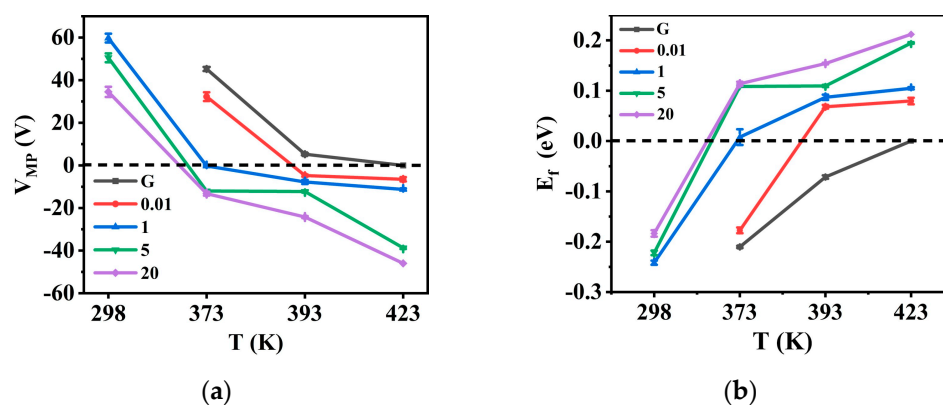


**Figure 6.** (a) Summarized  $V_g$  of MP on the transfer curves and (b)  $E_f$  (related to the MP position) of pristine G and CN-PPV-G samples casted from different concentrations before and after annealing 1 h at different temperatures. The dashed line in (a,b) indicates the  $V_g = 0$  and energy level of MP (set as reference point of  $E_f$ ), respectively. RT is around 298 K.

With the increment of annealing temperature to 393 K, MP ( $E_f$ ) of G and CN-PPV-G prepared from  $0.01 \text{ mg mL}^{-1}$  solution was displaced to a much left (up) position, but their left (up) movement during higher temperature treatment (423 K) is very small (Figures 5c,d and 6). Whereas for the CN-PPV-G fabricated from denser solutions ( $5 \text{ mg mL}^{-1}$  and  $20 \text{ mg mL}^{-1}$ ), MP ( $E_f$ ) shifting tendency is reversed, a small step from 373 K to 393 K but a large one from 393 K to 423 K. For the samples from  $1 \text{ mg mL}^{-1}$  solution, MP ( $E_f$ ) changing is roughly equivalent in these two annealing processes. Within expectation, the  $I_{ds}$  order in the output curves of Figures S6c and S6d is the same to that of the transfer curves at  $V_g = 0 \text{ V}$  in Figures 5c and 5d, respectively.

Overall, it can be seen that all of CN-PPV-G are in a  $n$ -doping state after 393 K annealing, and the doping effect was enhanced by the annealing at higher temperature (423 K) (Figure 6). Furthermore, the  $n$ -doping effect demonstrates a clear correlation with the concentration of CN-PPV solution. In detail, the  $n$ -doping effect in the CN-PPV-G samples from dilute solutions ( $0.01 \text{ mg mL}^{-1}$  and  $1 \text{ mg mL}^{-1}$ ) is insufficient in comparison with the samples from denser solutions ( $5 \text{ mg mL}^{-1}$  and  $20 \text{ mg mL}^{-1}$ ), which is consistent with the results revealed by AFM and SEM, the extreme thin, even noncontinuous film in the former two samples *vs* dense and continuous one in the latter two samples. In all the conditions (before and after annealing at different temperatures), the sequence of  $I_{ds}$  values determined from the transfer curves at  $V_g = 0 \text{ V}$  matches well with the one from output curves, indicating the high quality and reliability of our devices.

From the above analysis on the topography and electronic properties of hybrid films, it can be found that, in our tested range, the  $n$ -doping effect of CN-PPV to G layers can be enhanced via increment of thickness of CN-PPV part and temperature of post annealing.

### 2.3. Quick and Sensitive Detection of $\text{NO}_2$ Based on CN-PPV-G Films

$\text{NO}_2$  has a strong  $p$ -doping effect to G materials. The above tests indicate G layers can be doped to a very high  $n$ -doping state by CN-PPV film. Thus, CN-PPV-G hybrid films could be a very promising candidate for realizing effective detections to toxic  $\text{NO}_2$ . The summarized MP and  $E_f$  positions with solution concentrations and annealing temperatures in Figure 6 imply the solution suitable for fabricating  $\text{NO}_2$  sensing devices should not be lower than  $5 \text{ mg mL}^{-1}$  and the annealing temperature is 423 K. To realize active sensing,  $\text{NO}_2$  needs diffuse into CN-PPV film rapidly. If the film is too thick, it may slow down this diffusion process, thus causing the deterioration of sensing performances. Therefore, CN-PPV-G FET for detecting  $\text{NO}_2$  was fabricated with a  $5 \text{ mg mL}^{-1}$  solution and annealed at 423 K.

The transfer curves of CN-PPV-G transistors demonstrate immediate response to 50 ppm  $\text{NO}_2$  within 10 s (Figure 7a), which is an extremely high reacting speed (Table 1).

$\text{NO}_2$  shifts the MP of transfer curves to a right position because the  $n$ -doping effect is neutralized by the  $p$ -doping properties of  $\text{NO}_2$ . The right displacement of MP leads to the hole (electron)-dominated conductivity apparently being increased (depressed). As a result,  $I_{\text{sensing}}$ , defined as the alteration of  $I_{\text{ds}}$  with/without exposure to  $\text{NO}_2$  gas, is a lying-down S shape (Figure 7b). The data of response (R) calculated by normalizing  $I_{\text{sensing}}$  with  $I_{\text{ds}}$  of no exposure to  $\text{NO}_2$  follow the changing tendency of  $I_{\text{sensing}}$  (Figure 7c). Longer exposure time induces larger changing of transfer curves and higher values of  $I_{\text{sensing}}$  and R (Figure 7b,c), verifying that the alterations of the transfer curves come from the  $p$ -doping effect of  $\text{NO}_2$  indeed. Although the linear output curves of  $I_{\text{ds}}$  and  $I_{\text{sensing}}$  manifest obvious variations in  $\text{NO}_2$  environment as well (Figure S7), their detecting ability is not as good as that of the transfer curves due to lack of  $V_g$  tuning effect. As a consequence, we focused on the changing of transfer curves in the following experiments.

The concentration of  $\text{NO}_2$  was decreased gradually from 50 ppm to 100 ppb (Figures S8a,b and 7d, 25 ppm; Figures S8c,d and 7e, 1 ppm; Figures S8e,f and 7f, 100 ppb). At 25 ppm of  $\text{NO}_2$  (Figures S8a,b and 7d), our devices can still demonstrate a quick response within 10 s. The  $V_g$ -tuned changing tendency of  $I_{\text{ds}}$ ,  $I_{\text{sensing}}$  and R curves is similar to the corresponding one in 50 ppm  $\text{NO}_2$ . Decreasing the concentration of  $\text{NO}_2$  farther to 1 ppm (Figures S8c,d and 7e), the reliable sensing signal needs to be generated in a longer time although the curve shapes remain unchanged. Longer responding time in low concentration of  $\text{NO}_2$  environment is reasonable because the recognizable changing of electronic properties requires accumulating enough target molecules in CN-PPV-G film. However, in comparison with the data in a previous report (Table 1), 60 s–120 s reacting time to 1 ppm  $\text{NO}_2$  is still a very high speed.

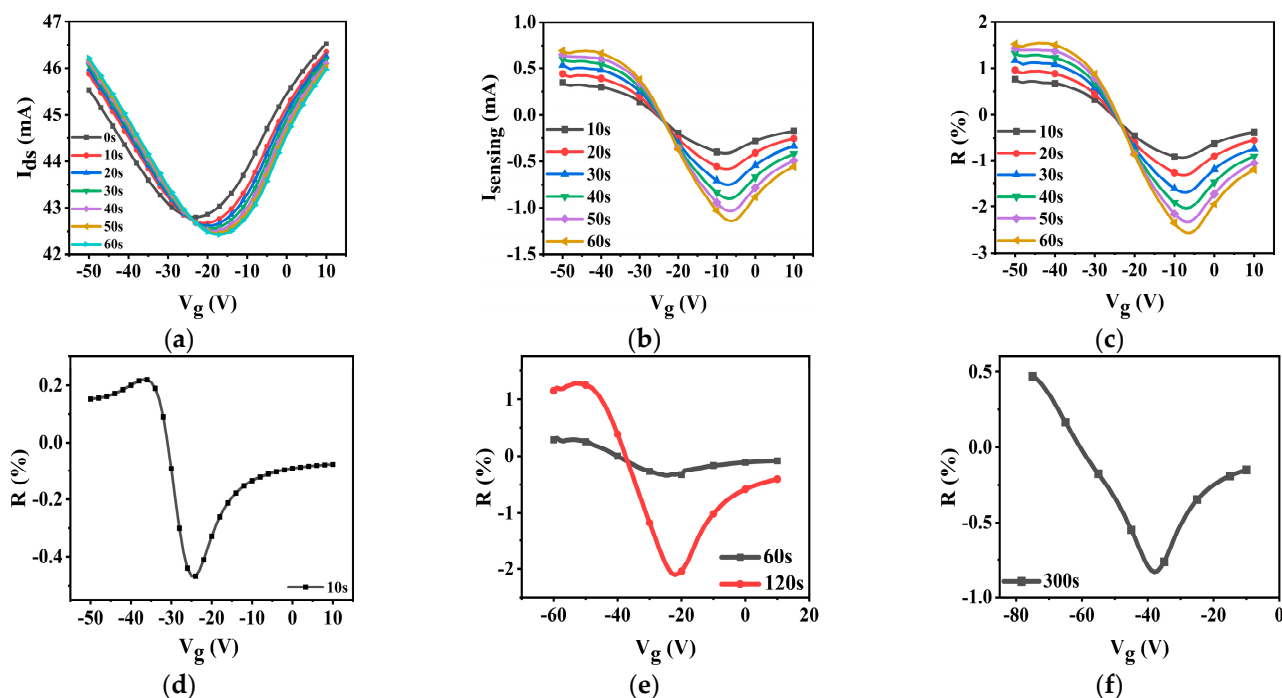


**Figure 7.**  $I_{\text{ds}}$  (a,  $V_{\text{ds}} = 1$  V),  $I_{\text{sensing}}$  (b) and (c)  $R$ - $V_g$  curves of CN-PPV-G transistors to 50 ppm  $\text{NO}_2$  in  $\text{N}_2$  environment;  $R$ - $V_g$  curves of CN-PPV-G transistors to 25 ppm (d), 1 ppm (e) and 100 ppb (f)  $\text{NO}_2$  in  $\text{N}_2$  environment. 0 s means before  $\text{NO}_2$  exposure.

**Table 1.** Response time of our CN-PPV-G sensors and the one in some previous reports.

	Environment	NO <sub>2</sub> Concentration			
		50 ppm	25 ppm	1 ppm	100 ppb
Response time	N <sub>2</sub>	10 s	10 s	60–120 s	300 s
	Dry air	10 s	10 s	60–120 s	300 s
References		~28 s to 25 ppm, MoSe <sub>2</sub> /G and ~70 s to 25 ppm, MoSe <sub>2</sub> , operated at RT [8]			
		~90 s to 50 ppm, Co (II) phthalocyanine/G quantum dot, operated at RT [9]			
		~300 s to 2 ppm, MoS <sub>2</sub> /RGO, operated at RT [20]			
		25 s to 25 ppm, PPV/porous silicon, operated at RT [28]			
		~300 s to 5 ppm, patterned G, operated above at RT (patterned G channel heated by bias voltage) [29]			
		~160 s to 5 ppm, ZnO/RGO, operated at RT [30]			
		420 s to 5 ppm, RGO, operated at RT [31]			
	~180 s to 200 ppm, GO, operated at RT [32]				
	~132 s to 50 ppm, ZnO/RGO aerogel, operated at RT [33]				

Successful detection of 100 ppb NO<sub>2</sub> within a reasonable responding time (300 s) was realized on our CN-PPV-G FET sensors (Figures S8e,f and 7f). Under this concentration, the positive peaks of  $I_{\text{sensing}}$  and R in the hole-conducting range cannot be recognized any more, but the prominent negative one originated from the depression of electron-dominated conductivity is conserved. The required detecting time for different concentration of NO<sub>2</sub> was listed in Table 1, revealing the ultrahigh responding speed of our sensors in comparison with the reported devices. The reliable  $I_{\text{sensing}}$  and R curves are well above background noise although they are not designed to achieve maximum as a tradeoff of fast responding.

For NO<sub>2</sub> sensors, quick responding capability is extremely important for alarming the exposure to this dangerous substance as early as possible to avoid serious damages to our health and environment in a short and long term. The reacting time of our sensors is 10 s at 25 ppm, which almost meets the demands of immediate alarming to 20 ppm NO<sub>2</sub> suggested by National Institute for Occupational Safety and Health (USA) [34]. Besides the very high reacting speed, LOD of CN-PPV-G NO<sub>2</sub> sensors is as low as 100 ppb (Figures S8e,f and 7f), lower than 200 ppb -the highest exposure concentration of NO<sub>2</sub> advised by American Conference of Governmental Industrial Hygienists [34]. These prominent sensing features indicate CN-PPV-G hybrid film is a promising candidate for developing commercial NO<sub>2</sub> sensors.

Furthermore, our CN-PPV-G NO<sub>2</sub> sensors exhibit excellent performances in dry air (21%O<sub>2</sub>/N<sub>2</sub>79%) environment as well. The transfer curves of  $I_{\text{ds}}$ ,  $I_{\text{sensing}}$  and R from 50 ppm to 100 ppb were provided in Figures 8 and S9. It can be found that the main features of  $I_{\text{ds}}$ ,  $I_{\text{sensing}}$  and R- $V_g$  curves under each concentration of NO<sub>2</sub> are the same as the corresponding one in N<sub>2</sub> atmosphere except the initial MP is displaced to a much right position. The *p*-doping effect of O<sub>2</sub> results in the shift of the initial MP locations. NO<sub>2</sub> was not introduced into the testing chamber until the transfer curves of hybrid films show negligible alterations in dry air. The remarkable operating speed and LOD of CN-PPV-G hybrids to NO<sub>2</sub> are not affected by the presence of O<sub>2</sub> (Table 1), unveiling the favorable characteristics of our CN-PPV-G NO<sub>2</sub> sensors further.

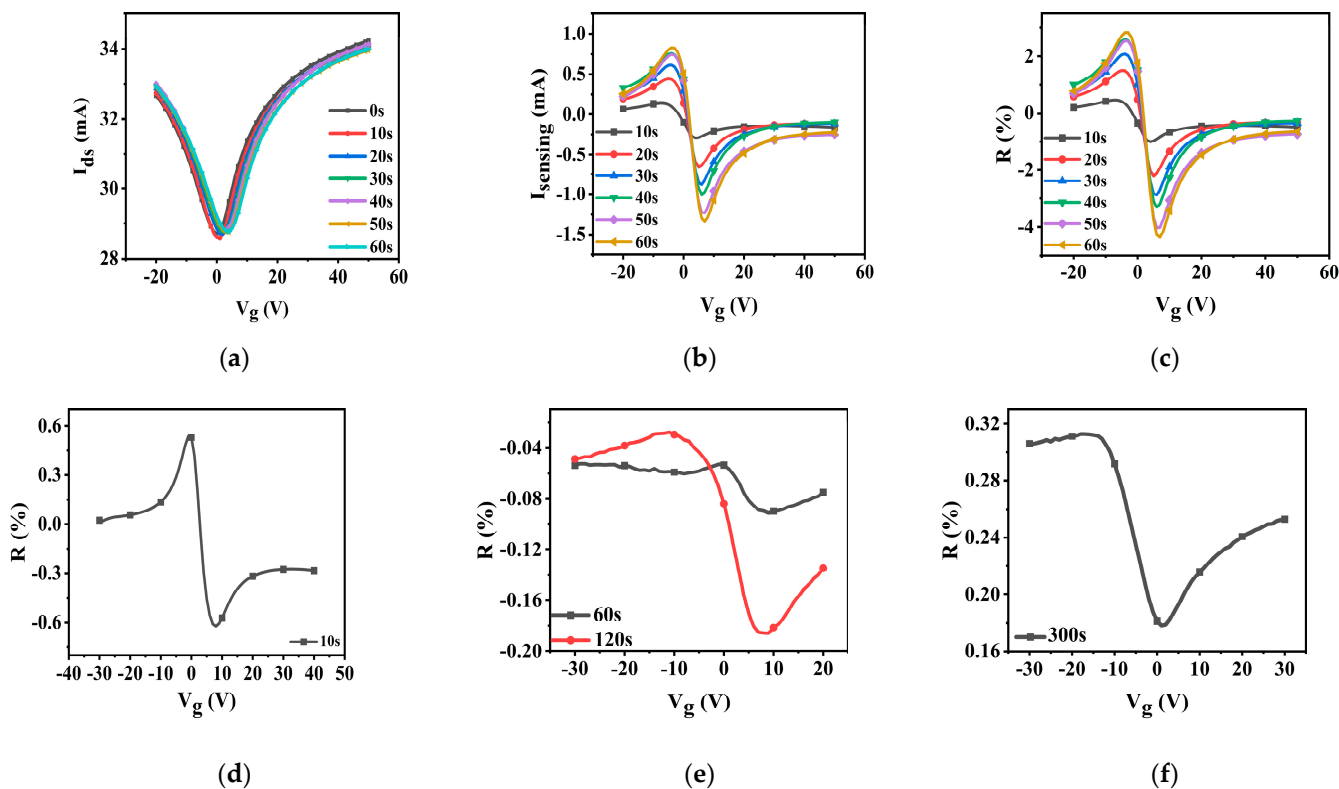


**Figure 8.**  $I_{ds}$  (a,  $V_{ds} = 1$  V),  $I_{sensing}$  (b) and (c)  $R-V_g$  curves of CN-PPV-G transistors to 50 ppm  $NO_2$  in dry air;  $R-V_g$  curves of CN-PPV-G transistors to 25 ppm (d), 1 ppm (e) and 100 ppb (f)  $NO_2$  in dry air. 0 s means before  $NO_2$  exposure.  $NO_2$  was not introduced into the testing chamber until the transfer curves of hybrid films show negligible alterations in dry air.

Our CN-PPV-G  $NO_2$  sensors can be used repeatedly (Figure 9). Adsorbed  $NO_2$  can be released via thermal annealing, thus, the hybrid films are refreshed. The CN-PPV-G hybrids demonstrate good stability during the sensing-refreshing cycles.

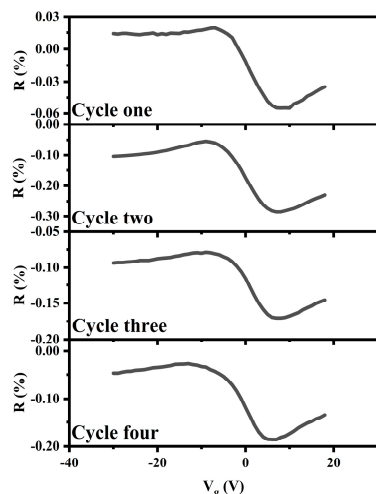


**Figure 9.**  $R-V_g$  ( $V_{ds} = 1$  V) curves of CN-PPV-G transistors in the several sensing-refreshing cycles. Testing conditions, 120 s data of 1 ppm  $NO_2$  in dry air.

### 3. Experiments and Methods

G on Cu foil (25  $\mu m$ , Alfa Aesar, Ward Hill, MA, USA) was prepared by chemical vapor deposition method using  $H_2$  and  $CH_4$ . Transferring G was performed under the assistance

of PMMA (poly(methyl methacrylate), 950 PMMA A4, MicroChem, Westborough, MA, USA) followed by repeatable rinsing by hot acetone and deionized water. Interdigitated Au electrodes with channel gap/width 200  $\mu\text{m}$  were deposited through thermal evaporation with a steel mask after G was transferred onto SiO<sub>2</sub> (300 nm)/Si chip. CN-PPV (HongKongJiSiEnBei International Trade Co., Limited, Hong Kong, China) in tetrahydrofuran (Sigma-Aldrich, Saint Louis, MO, USA, both used as received) was spin-coated on G after electrode preparation. The heating treatments of CN-PPV-G films and cooling down to room temperature were carried out in N<sub>2</sub> or Ar environment.

The hybrid films were characterized with atomic force microscopy (AFM, NTEGRA Prima), scanning electron microscopy (SEM, Hitachi, Regulus 8220, Ibaraki, Japan), Raman spectroscopy (Renishaw inVia) and grazing-incident wide angle X-ray scattering (GIWAXS) experiments (1W1A Diffuse-X-ray Scattering Station, Beijing Synchrotron Radiation Facility, BSRF-1W1A, Beijing, China). The devices were tested at room temperature in a glove box or small chamber designed specifically for gas sensor investigations with an outside source meter (Keithley 2612B). The flow of gases was controlled by mass flow meter.

The Fermi level ( $E_f$ , related to MP of the transfer curves) of CN-PPV-G samples was estimated by the  $V_g$  (MP) on the transfer curves and the following equation suggested in the previous reports [35,36]:

$$\Delta E_f = \hbar \times v_F \times ((\pi \times \epsilon_0 \times \epsilon_r / e) \times (V_g (\text{MP}) / d))^{1/2}$$

$\hbar$  is reduced Planck constant;  $v_F \approx 10^6 \text{ m s}^{-1}$ , is Fermi velocity of electrons in G;  $\epsilon_0$  and  $\epsilon_r$  ( $\approx 3.9$ ) is the vacuum permittivity and relative permittivity of SiO<sub>2</sub>, respectively;  $e$  is the absolute value of electronic charge;  $d \approx 300 \text{ nm}$ , is the thickness of SiO<sub>2</sub> layer.

$\Delta E_f$  is a positive (negative) value when  $V_g$  (MP) is a negative (positive) one, indicating  $E_f$  is above (below) the MP position.

#### 4. Conclusions

In this work, the strong  $n$ -doping effect of CN-PPV films to G sheets is unveiled. Thick film and high-temperature post annealing can enhance the doping effect. CN-PPV films are quasi amorphous and thermal annealing has no help on forming ordered arrangement. Heavily  $n$ -doped CN-PPV-G transistors demonstrate very quick and sensitive response to hazardous NO<sub>2</sub> gas in both N<sub>2</sub> and dry air atmosphere. The  $n$ -doping state is reduced by the adsorption of  $p$ -dopant NO<sub>2</sub>, causing the prompt alterations of transfer curves of CN-PPV-G transistors in a short time. Relying on this mechanism, CN-PPV-G transistors can react to 25 ppm NO<sub>2</sub> within 10 s, and LOD is as low as 100 ppb. These results suggest CN-PPV-G hybrid is a promising candidate for in situ monitoring the exposure of NO<sub>2</sub> and triggering immediate alerts when needed. A reacting time of 10 s at 25 ppm of NO<sub>2</sub> almost meets the demands of immediate alarming to 20 ppm NO<sub>2</sub> suggested by National Institute for Occupational Safety and Health (USA), and 100 ppb of LOD is lower than the highest exposure concentration of NO<sub>2</sub> (200 ppb) advised by American Conference of Governmental Industrial Hygienists. The remarkable detecting performances of our devices are not affected in dry air and can be restored through simple annealing treatment. This work also indicates that the transfer curves of transistors may react more promptly to the exposure of target substances and can be used to develop sensing devices designed specifically to meet the demand of quick responding whereas the smaller value of response is allowed as a tradeoff.

**Supplementary Materials:** The following supporting information can be downloaded at: <https://www.mdpi.com/article/10.3390/molecules28135054/s1>, Figure S1: AFM topography images of CN-PPV-G films prepared with the solution of 0.01 mg mL<sup>-1</sup> (a), 1 mg mL<sup>-1</sup> (b) and 20 mg mL<sup>-1</sup> (c) before and after 1 h thermal annealing at 373 K, 393 K and 423 K; Figure S2: SEM images of CN-PPV-G films prepared with the solution of 0.01 mg mL<sup>-1</sup> (a), 1 mg mL<sup>-1</sup> (b) and 20 mg mL<sup>-1</sup> (c) before and after 1 h thermal annealing at 373 K, 393 K and 423 K. Contrast and brightness of zoom-in images were post adjusted to clearly show the topographical target which are not easily recognized

in the small-size original micrographs; Figure S3: (a,b) GIWAXS patterns collected on CN-PPV-G films prepared from 5 mg mL<sup>-1</sup> before and after annealed 1 h at 373 K and 393 K, respectively. The first dot in the z direction of each image is not a signal that can be reasonably generated by our CN-PPV-G films. So we discarded the corresponding peak in the fitting profiles (Figure S4); Figure S4: (a-d) The z direction fitting profiles of CN-PPV-G films prepared from 5 mg mL<sup>-1</sup> before and after annealed 1 h at 373 K, 393 K and 423 K, respectively. In each profile, the first peak produced by the first dot in GIWAXS pattern is discarded because the first dot is not a signal that can be reasonably generated by our CN-PPV-G films; Figure S5: Raman spectroscopy of CN-PPV-G casted from 0.01 mg mL<sup>-1</sup> solution after annealing 1 h at 423 K; Figure S6: The output curves of pristine G and CN-PPV-G samples casted from different concentrations before (a) and after annealing 1 h at 373 K (b), 393 K (c) and 423 K (d); Figure S7: I<sub>ds</sub> (a) and I<sub>sensing</sub> (b) -V<sub>ds</sub> curves of CN-PPV-G transistors exposure to 50 ppm NO<sub>2</sub> in N<sub>2</sub> environment at V<sub>g</sub> = 0 V. 0 s means before NO<sub>2</sub> exposure; Figure S8: I<sub>ds</sub> (a, V<sub>ds</sub> = 1 V) and I<sub>sensing</sub> (b)-V<sub>g</sub> curves of CN-PPV-G transistors to 25 ppm NO<sub>2</sub> in N<sub>2</sub> environment; I<sub>ds</sub> (c, V<sub>ds</sub> = 1 V) and I<sub>sensing</sub> (d)-V<sub>g</sub> curves of CN-PPV-G transistors to 1 ppm NO<sub>2</sub> in N<sub>2</sub> environment; I<sub>ds</sub> (e, V<sub>ds</sub> = 1 V) and I<sub>sensing</sub> (f)-V<sub>g</sub> curves of CN-PPV-G transistors to 100 ppb NO<sub>2</sub> in N<sub>2</sub> environment. 0 s means before NO<sub>2</sub> exposure; Figure S9: I<sub>ds</sub> (a, V<sub>ds</sub> = 1 V) and I<sub>sensing</sub> (b)-V<sub>g</sub> curves of CN-PPV-G transistors to 25 ppm NO<sub>2</sub> in dry air; I<sub>ds</sub> (c, V<sub>ds</sub> = 1 V) and I<sub>sensing</sub> (d)-V<sub>g</sub> curves of CN-PPV-G transistors to 1 ppm NO<sub>2</sub> in in dry air; I<sub>ds</sub> (e, V<sub>ds</sub> = 1 V) and I<sub>sensing</sub> (f)-V<sub>g</sub> curves of CN-PPV-G transistors to 100 ppb NO<sub>2</sub> in dry air. 0 s means before NO<sub>2</sub> exposure. NO<sub>2</sub> was not introduced into the testing chamber until the transfer curves of hybrid films show negligible alterations in dry air.

**Author Contributions:** Conceptualization, Z.-Y.Y.; Investigation, S.-W.S., Q.-M.W. and M.Y.; Writing—original draft, S.-W.S. and Q.-M.W.; Writing—review & editing, Z.-Y.T. and Z.-Y.Y.; Supervision, Z.-Y.Y. All authors have read and agreed to the published version of the manuscript.

**Funding:** This work is funded in part by the National Natural Science Foundation of China (grants 22272177, 21872146), Fundamental Research Funds for the Central Universities and University of Chinese Academy of Sciences.

**Institutional Review Board Statement:** Not applicable.

**Informed Consent Statement:** Not applicable.

**Data Availability Statement:** Not applicable.

**Acknowledgments:** The authors gratefully acknowledge the cooperation of the beamline scientists at BSRF-1W1A.

**Conflicts of Interest:** The authors declare no conflict of interest.

**Sample Availability:** Not applicable.

## References

1. Lv, Y.-K.; Li, Y.-Y.; Zhou, R.-H.; Pan, Y.-P.; Yao, H.-C.; Li, Z.-J. N-Doped Graphene Quantum Dot-Decorated Three-Dimensional Ordered Macroporous In<sub>2</sub>O<sub>3</sub> for NO<sub>2</sub> Sensing at Low Temperatures. *ACS Appl. Mater. Interfaces* **2020**, *12*, 34245–34253. [[CrossRef](#)] [[PubMed](#)]
2. Cao, P.; Cai, Y.; Pawar, D.; Navale, S.T.; Rao, C.N.; Han, S.; Xu, W.; Fang, M.; Liu, X.; Zeng, Y.; et al. Down to Ppb Level NO<sub>2</sub> Detection by ZnO/RGO Heterojunction Based Chemiresistive Sensors. *Chem. Eng. J.* **2020**, *401*, 125491. [[CrossRef](#)]
3. Yan, X.; Wu, Y.; Li, R.; Shi, C.; Moro, R.; Ma, Y.; Ma, L. High-Performance UV-Assisted NO<sub>2</sub> Sensor Based on Chemical Vapor Deposition Graphene at Room Temperature. *ACS Omega* **2019**, *4*, 14179–14187. [[CrossRef](#)]
4. Bag, A.; Lee, N.-E. Gas Sensing with Heterostructures Based On Two Dimensional Nanostructured Materials: A Review. *J. Mater. Chem. C* **2019**, *7*, 13367–13383. [[CrossRef](#)]
5. Chang, C.; Chen, W.; Chen, Y.; Chen, Y.; Ding, F.; Fan, C.; Fan, H.J.; Fan, Z.; Gong, C.; et al. Recent Progress on Two-Dimensional Materials. *Acta Phys. Chim. Sin.* **2021**, *37*, 2108017. [[CrossRef](#)]
6. Alzate-Carvajal, N.; Luican-Mayer, A. Functionalized Graphene Surfaces for Selective Gas Sensing. *ACS Omega* **2020**, *5*, 21320–21329. [[CrossRef](#)] [[PubMed](#)]
7. Qu, G.; Fan, G.; Zhou, M.; Rong, X.; Li, T.; Zhang, R.; Sun, J.; Chen, D. Graphene-Modified ZnO Nanostructures for Low-Temperature NO<sub>2</sub> Sensing. *ACS Omega* **2019**, *4*, 4221–4232. [[CrossRef](#)]
8. Rathi, K.; Pal, K. Fabrication of MoSe<sub>2</sub>-Graphene Hybrid Nanoflakes for Toxic Gas Sensor with Tunable Sensitivity. *Adv. Mater. Interfaces* **2020**, *7*, 2000140.

9. Jiang, W.; Chen, X.; Wang, T.; Li, B.; Zeng, M.; Yang, J.; Hu, N.; Su, Y.; Zhou, Z.; Yang, Z. Enhancing Room-Temperature NO<sub>2</sub> Gas Sensing Performance Based on a Metal Phthalocyanine/Graphene Quantum Dot Hybrid Material. *RSC Adv.* **2021**, *11*, 5618–5628. [[CrossRef](#)]
10. Srivastava, S.; Pal, P.; Sharma, D.K.; Kumar, T.D.S.S.; Gupta, B.K. Ultrasensitive Boron-Nitrogen-Codoped CVD Graphene-Derived NO<sub>2</sub> Gas Sensor. *ACS Mater. Au* **2022**, *2*, 356–366. [[CrossRef](#)]
11. Zhang, L.; Zhang, J.; Huang, Y.; Xu, H.; Zhang, X.; Lu, H.; Xu, K.; Chu, P.K.; Ma, F. Stability and Sensing Enhancement by Nanocubic CeO<sub>2</sub> with {100} Polar Facets on Graphene for NO<sub>2</sub> at Room Temperature. *ACS Appl. Mater. Interfaces* **2020**, *12*, 4722–4731. [[CrossRef](#)]
12. Lee, S.W.; Lee, W.; Hong, Y.; Lee, G.; Yoon, D.S. Recent Advances in Carbon Material-Based NO<sub>2</sub> Gas Sensors. *Sens. Actuators B Chem.* **2018**, *255*, 1788–1804. [[CrossRef](#)]
13. Wang, Y.; Liu, L.; Sun, F.; Li, T.; Zhang, T.; Qin, S. Humidity-Insensitive NO<sub>2</sub> Sensors Based on SnO<sub>2</sub>/rGO Composites. *Front. Chem.* **2021**, *9*, 681313. [[CrossRef](#)]
14. Cao, P.; Cai, Y.; Pawar, D.; Han, S.; Xu, W.; Fang, M.; Liu, X.; Zeng, Y.; Liu, W.; Lu, Y.; et al. Au@ZnO/RGO Nanocomposite-Based Ultra-Low Detection Limit Highly Sensitive and Selective NO<sub>2</sub> Gas Sensor. *J. Mater. Chem. C* **2022**, *10*, 4295–4305. [[CrossRef](#)]
15. Xia, Y.; Wang, J.; Xu, J.-L.; Li, X.; Xie, D.; Xiang, L.; Komarneni, S. Confined Formation of Ultrathin ZnO Nanorods/Reduced Graphene Oxide Mesoporous Nanocomposites for High-Performance Room-Temperature NO<sub>2</sub> Sensors. *ACS Appl. Mater. Interfaces* **2016**, *8*, 35454–35463. [[CrossRef](#)] [[PubMed](#)]
16. Wang, Z.; Gao, S.; Fei, T.; Liu, S.; Zhang, T. Construction of ZnO/SnO<sub>2</sub> Heterostructure on Reduced Graphene Oxide for Enhanced Nitrogen Dioxide Sensitive Performances at Room Temperature. *ACS Sens.* **2019**, *4*, 2048–2057. [[CrossRef](#)]
17. Lee, S.W.; Jung, H.G.; Kim, I.; Lee, D.; Kim, W.; Kim, S.H.; Lee, J.H.; Park, J.; Lee, J.H.; Lee, G.; et al. Highly Conductive and Flexible Dopamine-Graphene Hybrid Electronic Textile Yarn for Sensitive and Selective NO<sub>2</sub> Detection. *ACS Appl. Mater. Interfaces* **2020**, *12*, 46629–46638. [[CrossRef](#)] [[PubMed](#)]
18. Chi, H.; Xu, Z.; Duan, X.; Yang, J.; Wang, F.; Li, Z. High-Performance Colorimetric Room-Temperature NO<sub>2</sub> Sensing Using Spin-Coated Graphene/Polyelectrolyte Reflecting Film. *ACS Appl. Mater. Interfaces* **2019**, *11*, 32390–32397. [[CrossRef](#)]
19. Lee, S.W.; Lee, W.; Kim, I.; Lee, D.; Park, D.; Kim, W.; Park, J.; Lee, J.H.; Lee, G.; Yoon, D.S. Bio-Inspired Electronic Textile Yarn-Based NO<sub>2</sub> Sensor Using Amyloid-Graphene Composite. *ACS Sens.* **2021**, *6*, 777–785. [[CrossRef](#)] [[PubMed](#)]
20. Yi, N.; Cheng, Z.; Li, H.; Yang, L.; Zhu, J.; Zheng, X.; Chen, Y.; Liu, Z.; Zhu, H.; Cheng, H. Stretchable, Ultrasensitive, and Low-Temperature NO<sub>2</sub> Sensors Based on MoS<sub>2</sub>@rGO Nanocomposites. *Mater. Today Phys.* **2020**, *15*, 100265. [[CrossRef](#)]
21. Ghasemi, F. Vertically Aligned Carbon Nanotubes, MoS<sub>2</sub>-rGO Based Optoelectronic Hybrids for NO<sub>2</sub> Gas Sensing. *Sci. Rep.* **2020**, *10*, 11306. [[CrossRef](#)]
22. Anichini, C.; Czepa, W.; Pakulski, D.; Aliprandi, A.; Ciesielski, A.; Samor, P. Chemical Sensing With 2D Materials. *Chem. Soc. Rev.* **2018**, *47*, 4860–4908. [[CrossRef](#)] [[PubMed](#)]
23. Yang, C.-M.; Chen, T.-C.; Yang, Y.-C.; Meyyappan, M. Annealing Effect on UV-Illuminated Recovery in Gas Response of Graphene-Based NO<sub>2</sub> Sensors. *RSC Adv.* **2019**, *9*, 23343–23351. [[CrossRef](#)] [[PubMed](#)]
24. Kumar, S.; Kaushik, S.; Pratap, R.; Raghavan, S. Graphene on Paper: A Simple, Low-Cost Chemical Sensing Platform. *ACS Appl. Mater. Interfaces* **2015**, *7*, 2189–2194. [[CrossRef](#)] [[PubMed](#)]
25. Choi, H.; Choi, J.S.; Kim, J.-S.; Choe, J.-H.; Chung, K.H.; Shin, J.-W.; Kim, J.T.; Youn, D.H.; Kim, K.C.; Lee, J.I.; et al. Flexible and Transparent Gas Molecule Sensor Integrated with Sensing and Heating Graphene Layers. *Small* **2014**, *10*, 3685–3691. [[CrossRef](#)]
26. Schedin, F.; Geim, A.K.; Morozov, S.V.; Hill, E.W.; Blake, P.; Katsnelson, M.I.; Novoselov, K.S. Detection Of Individual Gas Molecules Adsorbed on Graphene. *Nat. Mater.* **2007**, *6*, 652–655. [[CrossRef](#)]
27. Banerjee, J.; Dutta, K. A Short Overview on the Synthesis, Properties and Major Applications of Poly(p-Phenylene Vinylene). *Chem. Pap.* **2021**, *75*, 5139–5151. [[CrossRef](#)]
28. Abbas, N.K.; Ibrahim, I.M.; Saleh, M.A. Characteristics of MEH-PPV/Si and MEH-PPV/PS Heterojunctions as NO<sub>2</sub> Gas Sensors. *Silicon* **2018**, *10*, 1345–1350. [[CrossRef](#)]
29. Kim, Y.H.; Kim, S.J.; Kim, Y.-J.; Shim, Y.-S.; Kim, S.Y.; Hong, B.H.; Jang, H.W. Self-Activated Transparent All-Graphene Gas Sensor with Endurance to Humidity and Mechanical Bending. *ACS Nano* **2015**, *9*, 10453–10460. [[CrossRef](#)]
30. Liu, S.; Yu, B.; Zhang, H.; Fei, T.; Zhan, T. Enhancing NO<sub>2</sub> Gas Sensing Performances at Room Temperature Based on Reduced Graphene Oxide-ZnO Nanoparticles Hybrids. *Sens. Actuators B Chem.* **2014**, *202*, 272–278. [[CrossRef](#)]
31. Su, P.-G.; Shieh, H.-C. Flexible NO<sub>2</sub> Sensors Fabricated By Layer-by-Layer Covalent Anchoring and In Situ Reduction of Graphene Oxide. *Sens. Actuators B Chem.* **2014**, *190*, 865–872. [[CrossRef](#)]
32. Yang, G.; Lee, C.; Kim, J.; Ren, F.; Pearton, S.J. Flexible Graphene-Based Chemical Sensors on Paper Substrates. *Phys. Chem. Chem. Phys.* **2013**, *15*, 1798–1801. [[CrossRef](#)]
33. Liu, X.; Sun, J.; Zhang, X. Novel 3D Graphene Aerogel-ZnO Composites as Efficient Detection for NO<sub>2</sub> at Room Temperature. *Sens. Actuators B Chem.* **2015**, *211*, 220–226. [[CrossRef](#)]
34. Yuan, W.; Huang, L.; Zhou, Q.; Shi, G. Ultrasensitive and Selective Nitrogen Dioxide Sensor Based on Self-Assembled Graphene/Polymer Composite Nanofibers. *ACS Appl. Mater. Interfaces* **2014**, *6*, 17003–17008. [[CrossRef](#)] [[PubMed](#)]

35. Matkovic, A.; Kratzer, M.; Kaufmann, B.; Vujin, J.; Gajic, R.; Teichert, C. Probing Charge Transfer Between Molecular Semiconductors and Graphene. *Sci. Rep.* **2017**, *7*, 9544. [[CrossRef](#)] [[PubMed](#)]
36. Yu, M.; Chen, Y.; Chen, Y.-G.; Yang, Z.-Y.; Zhang, W.-F.; Yu, G. Synergy Between Fermi Level of Graphene and Morphology of Polymer Film Allows Broadband or Wavelength-Sensitive Photodetection. *Adv. Mater. Interfaces* **2021**, *8*, 2100770. [[CrossRef](#)]

**Disclaimer/Publisher's Note:** The statements, opinions and data contained in all publications are solely those of the individual author(s) and contributor(s) and not of MDPI and/or the editor(s). MDPI and/or the editor(s) disclaim responsibility for any injury to people or property resulting from any ideas, methods, instructions or products referred to in the content.